

G-iMUSIC: Greedy Iterative MUSIC Algorithms for Multi-Target DoA Estimation

Martin Willame, *Graduated Student Member, IEEE*, Gilles Monnoyer, *Member, IEEE*,
François Horlin, *Fellow, IEEE* and Jérôme Louveaux, *Fellow, IEEE*

Abstract—This paper presents novel algorithms for multi-target direction-of-arrival (DoA) estimation in array signal processing. Although the maximum likelihood estimator (MLE) asymptotically attains the Cramér-Rao bound, its exponential complexity motivates practical alternatives, such as greedy or subspace-based methods. In this context, greedy methods such as orthogonal matching pursuit (OMP) and orthogonal least squares (OLS) are sensitive to early selection errors, especially for angularly proximate targets, whereas subspace-based methods such as multiple signal classification (MUSIC) present angular super-resolution capabilities but degrade under strong inter-target signal correlation. To overcome these limitations, we propose two greedy iterative MUSIC (G-iMUSIC) algorithms, namely OMP-iMUSIC and OLS-iMUSIC, derived from a unified framework that links subspace and greedy estimations. Unlike prior iMUSIC approaches, the proposed methods require only one initial eigen value decomposition (EVD) and avoid computing eigendecomposition at each iteration. They also admit Fast Fourier Transform (FFT)-accelerated implementations for uniform linear arrays (ULAs), enabling low-complexity operation. Monte Carlo simulations demonstrate improved detection and precision over conventional OMP, OLS, and MUSIC, as well as reduced processing time compared to greedy baselines. Finally, we introduce diagnostic metrics that interpret performance across signal correlation and angular proximity regimes, supporting generalization beyond the specific orthogonal frequency-division multiplexing (OFDM) radar scenario considered.

Index Terms—iMUSIC, direction-of-arrival, greedy, MUSIC, OMP, OLS

I. INTRODUCTION

MULTI-target direction-of-arrival (DoA) estimation remains a central problem in array signal processing, with applications across the radar, sonar, wireless communications, and acoustics fields [1], [2]. Given noisy measurements collected by a sensor array, the objective is to recover the set of source directions with high resolution and reliability. Although this objective is conceptually simple, practical performance is fundamentally constrained by a limited array aperture, finite sample support, low signal-to-noise ratio (SNR) and inter-target correlation, while real-time operation further imposes strict computational requirements. In this paper, we study algorithmic designs that jointly improve statistical robustness, angular resolution, and computational efficiency for multi-target DoA estimation.

This paper was submitted on the 26th of May, 2026. Martin Willame is with the Université Catholique de Louvain (UCLouvain) and the Université Libre de Bruxelles (ULB). Gilles Monnoyer and Jérôme Louveaux are with the UCLouvain (e-mails: {martin.willame, gilles.monnoyer, jerome.louveaux@uclouvain.be}). François Horlin is with the ULB (e-mails: francois.horlin@ulb.be).

A. Related Work and Motivation

To motivate our contribution, we review state-of-the-art methods for multi-target DoA estimation and highlight their trade-offs. Table I summarizes these methods qualitatively. The maximum likelihood estimator (MLE) is asymptotically efficient under additive white Gaussian noise (AWGN) by reaching the Cramér-Rao bound as the number of observations grows [2]–[4]. However, it leads to a non-convex least-squares optimization problem whose complexity scales exponentially with the number of targets, limiting its practical use.

To reduce this complexity, greedy methods such as orthogonal matching pursuit (OMP) [5], [6] and orthogonal least squares (OLS) [7], [8] provide efficient approximations [1], [9]. Greedy algorithms iteratively build the solution by selecting one candidate DoA at a time, based on a selection criterion that approximates the MLE. While OLS generally provides more accurate approximations to MLE solutions [1], [10], OMP remains popular in radar because of its lower cost. When the targets present angularly proximate DoA, OLS offers clear gains, as shown both empirically [11] and theoretically [12], [13]. Nevertheless, greedy methods remain sensitive to early selection steps, whose capacity to resolve angularly proximate targets is constrained by the Rayleigh limit [14]. This can yield erroneous first estimates that propagate errors across iterations.

Subspace methods, notably multiple signal classification (MUSIC) and weighted MUSIC (WMUSIC), provide a complementary paradigm for DoA estimation [15]–[18]. Such methods exploit information in the signal structure to achieve angular super-resolution, defined as the ability to resolve closely spaced targets beyond the Rayleigh limit in a single step. Empirical studies indicate that MUSIC often surpasses WMUSIC [16], showing the superiority of unweighted subspace methods. However, subspace methods degrade when target signals are highly correlated [1].

Consequently, prior work has proposed iterative MUSIC (iMUSIC) variants [19]–[23], either through successive greedy detections [19], [20] or iterative refinement of all estimates [21]–[23]. Yet these approaches share two key limitations: they lack a principled statistical foundation, and they typically require repeated eigen value decomposition (EVD) at each iteration. The former can limit performance, while the latter is costly for real-time operation.

B. Main Contributions

To address these limitations, we propose two greedy iterative MUSIC (G-iMUSIC) methods—**OMP-iMUSIC** and **OLS-iMUSIC**—that combine the greedy frameworks of OMP

TABLE I
QUALITATIVE COMPARISON OF STATE-OF-THE-ART MULTI-TARGET DOA ESTIMATION METHODS AND THE PROPOSED iMUSIC VARIANTS.

Method	DoA References	Model	Estimation Strategy	Resolution	Angular Proximity Handling	Signal Correlation Handling	Computational Complexity	Key Limitation
MLE	[2], [4]	Parametric	Multidimensional Search	Optimal	Optimal	Optimal	Very high	Nonlinear optimization
OMP	[1], [13]	Sparse	Iterative greedy pursuit	Angular Rayleigh Limit	Average	Good	Low	Poor for angularly proximate targets
OLS	[1], [13]	Sparse	Iterative greedy pursuit	Angular Rayleigh Limit	Good	Very Good	Moderate	Poor in first steps for angularly proximate targets
MUSIC	[2], [15]	Subspace	Monodimensional Search	Super Resolution	Very Good	Bad	Very Low	Poor for correlated signals
OMP-iMUSIC	This work	Subspace & Sparse	Iterative greedy pursuit	Super Resolution	Good	Good	Very Low	Lower Performance than OLS-iMUSIC
OLS-iMUSIC	This work	Subspace & Sparse	Iterative greedy pursuit	Super Resolution	Very Good	Very Good	Low	Higher Complexity than OMP-iMUSIC

and OLS, with the subspace-based approach of MUSIC. Table I qualitatively compares the proposed algorithms with state-of-the-art methods. Our main contributions are:

- 1) **Greedy iterative MUSIC algorithms with improved estimation performance:** We develop two G-iMUSIC methods for multi-target DoA estimation, along with their weighted iMUSIC variants. Unlike existing iterative MUSIC heuristics, these methods rely on a unified framework that links subspace estimation and greedy optimization. The proposed algorithms achieve better localization performance than the subspace-based MUSIC methods and their greedy OMP and OLS counterparts while exhibiting lower computational complexity.
- 2) **Single-EVD design with FFT-accelerated implementation:** A central distinction from prior iMUSIC methods is that, in the proposed unified framework, G-iMUSIC algorithms are shown to avoid repeated EVD. Instead, they require only one initial EVD to estimate the signal and noise subspaces, and then iteratively update them using efficient updates. In addition, we introduce Fast Fourier Transform (FFT)-accelerated implementations in uniform linear array (ULA) settings for OLS and the proposed G-iMUSIC variants, extending such acceleration beyond existing MUSIC and OMP implementations. As a result, these design choices substantially reduce complexity and support real-time radar operation under strict latency constraints.
- 3) **Comprehensive complexity and performance characterization:** We provide a detailed theoretical complexity analysis together with extensive Monte Carlo simulations benchmarked against state-of-the-art methods. This study characterizes operational regimes as functions of key radar parameters and identifies where G-iMUSIC methods provide the largest gains.
- 4) **Practical passive OFDM radar validation with diagnostic metrics:** We validate the proposed G-iMUSIC algorithms in a practical passive orthogonal frequency-division multiplexing (OFDM) radar scenario without decoding unknown data symbols. Beyond this use case, the methods can be applied to other sensing scenarios. To support this extension, we introduce two diagnostic metrics: the *steering-vector cor-*

relation metric (\mathcal{T}) and the *signal correlation metric* (\mathcal{S}), which quantify the mean inter-target angular proximity and signal correlation, respectively. We then interpret performance through these metrics to provide scenario-agnostic guidance.

C. Paper Organization

The remainder of this paper is organized as follows. Section II introduces the system model. Section III reviews state-of-the-art algorithms for multi-target DoA estimation. Section IV presents the proposed G-iMUSIC algorithms. Section V details FFT accelerations in ULA settings. Section VI provides a comprehensive complexity analysis. Section VII demonstrates performance gains through extensive Monte Carlo simulations. Finally, Section VIII concludes the paper.

D. Mathematical Notation

Scalars, vectors, and matrices are denoted by a , \mathbf{a} , and \mathbf{A} , respectively. In the estimation context, θ , $\hat{\theta}$, and $\tilde{\theta}$ denote the true, candidate, and estimated values of a parameter. The sets of real and complex numbers are denoted by \mathbb{R} and \mathbb{C} . The trace, transpose, Hermitian transpose, and Moore-Penrose pseudoinverse operators are denoted by $\text{Tr}\{\mathbf{A}\}$, \mathbf{A}^T , \mathbf{A}^\dagger , and \mathbf{A}^\dagger , respectively. The vectorization operator that stacks all columns of a matrix is denoted by $\text{vec}(\mathbf{A})$. For a positive semidefinite matrix \mathbf{A} , its square-root matrix is denoted by $\mathbf{A}^{1/2}$ such that $\mathbf{A}^{1/2}(\mathbf{A}^{1/2})^\dagger = \mathbf{A}$. The identity matrix is denoted by $\mathbf{I}_M \in \mathbb{R}^{M \times M}$. The vector ℓ_2 norm and the matrix Frobenius norm are denoted by $\|\mathbf{a}\|_2$ and $\|\mathbf{A}\|_F$, while $\|\mathbf{A}\|_{2,c}$ denotes the column-wise ℓ_2 norm.

II. SYSTEM MODEL

In order to ground the proposed algorithms in a concrete application scenario, we consider a passive radar (PR) system designed to estimate the DoA of multiple targets using the reflected signals transmitted by an access point (AP). The AP and the PR can be either co-located (monostatic configuration)

or spatially separated (bistatic configuration). The single-antenna AP transmits an OFDM downlink signal that the passive receiver captures using a ULA of M antennas with an antenna spacing of Δ_d . The AP transmits a sequence of D OFDM data symbols, separated by T seconds. Each OFDM symbol contains Q subcarriers with uniform spacing Δ_f . The first subcarrier has frequency f_c and corresponding wavenumber $k_c \triangleq 2\pi f_c/c$, where c denotes the speed of light. The transmitted complex data symbol for the d^{th} OFDM symbol ($d \in \{0, \dots, D-1\}$) and q^{th} subcarrier ($q \in \{0, \dots, Q-1\}$) is denoted as $s_{d,q} \in \mathbb{C}$. These symbols remain unknown to the passive receiver.

The PR objective is to estimate the DoA of K targets within the coverage area. We define the true DoA of the k^{th} target as $\theta_k \in [-\pi/2, \pi/2]$. Collecting all target DoAs, we define the DoA vector $\Theta = [\theta_1 \dots \theta_K]^T \in \mathbb{R}^{K \times 1}$. DoAs measure the angle between the incoming wavefront and the normal vector of the receiver antenna array. Under the far-field assumption for all targets with respect to the receiver, the DoA steering vector $\mathbf{a}(\theta) \in \mathbb{C}^{M \times 1}$ and the corresponding steering matrix $\mathbf{A}(\Theta) \in \mathbb{C}^{M \times K}$ are defined as

$$\mathbf{a}(\theta) = [1 \ e^{jk_c \Delta_d \sin(\theta)} \dots \ e^{jk_c \Delta_d \sin(\theta)(M-1)}]^T, \quad (1)$$

$$\mathbf{A}(\Theta) = [\mathbf{a}(\theta_1) \dots \mathbf{a}(\theta_K)]. \quad (2)$$

We ground the channel model on the following assumptions: first, only single-bounce multipath signals contribute significantly to the observed channel; second, the receiver achieves perfect timing and frequency synchronization using the transmitted preamble. Under these assumptions, the channel for the d^{th} OFDM symbol and q^{th} subcarrier is expressed as $\mathbf{h}_{d,q}(\Theta, \beta_{d,q}) = \mathbf{A}(\Theta) \beta_{d,q}$, with,

$$\beta_{d,q} = [\beta_{d,q,1} \dots \beta_{d,q,K}]^T, \in \mathbb{C}^{K \times 1}, \quad (3)$$

$$\beta_{d,q,k} = \alpha_k e^{-j2\pi k_c \tau_k} e^{-j2\pi \Delta_f \tau_k q} e^{j2\pi f_k d/DT}, \in \mathbb{C}. \quad (4)$$

where the complex channel coefficient vector $\beta_{d,q}$ captures, for each target k , the path loss, the radar cross-section and the propagation phase (all encoded in $\alpha_k \in \mathbb{C}$), the range-induced phase shift (τ_k), and the Doppler shift (f_k) [24]. The model characterizing the received signal $\mathbf{y}_{d,q} \in \mathbb{C}^{M \times 1}$ at the PR is given by

$$\mathbf{y}_{d,q} = \mathbf{h}_{d,q}(\Theta, \beta_{d,q}) s_{d,q} + \mathbf{n}_{d,q} = \mathbf{A}(\Theta) \beta'_{d,q} + \mathbf{n}_{d,q}, \quad (5)$$

where $\beta'_{d,q} \triangleq \beta_{d,q} s_{d,q} \in \mathbb{C}^{K \times 1}$ represents the channel coefficients modulated by the unknown data symbol, and $\mathbf{n}_{d,q} \in \mathbb{C}^{M \times 1}$ denotes the AWGN contribution. Each noise vector $\mathbf{n}_{d,q} \stackrel{\text{i.i.d.}}{\sim} \mathcal{CN}(\mathbf{0}, \sigma^2 \mathbf{I}_M)$ is an independent and identically distributed (i.i.d.) circularly symmetric complex Gaussian random vector with zero mean and diagonal covariance matrix. The corresponding SNR is defined as

$$\text{SNR} = \frac{\frac{1}{K} \sum_{k=1}^K |\alpha_k|^2}{\sigma^2}. \quad (6)$$

With this definition, the SNR is dominated by the strongest target, which is also the "easiest" to detect. The received signal matrix $\mathbf{Y} = [\mathbf{y}_{0,0} \dots \mathbf{y}_{D-1,Q-1}]$ is expressed by juxtaposing all observation vectors as

$$\mathbf{Y} = \mathbf{A}(\Theta) \mathbf{B}' + \mathbf{N}, \in \mathbb{C}^{M \times DQ}, \quad (7)$$

where the modulated channel coefficient and noise matrices are defined as

$$\mathbf{B}' = [\beta'_{0,0} \dots \beta'_{D-1,Q-1}], \in \mathbb{C}^{K \times DQ}, \quad (8)$$

$$\mathbf{N} = [\mathbf{n}_{0,0} \dots \mathbf{n}_{D-1,Q-1}], \in \mathbb{C}^{M \times DQ}. \quad (9)$$

III. STATE-OF-THE-ART METHODS FOR MULTI-TARGET DOA ESTIMATION

This section reviews the main state-of-the-art DoA estimators and provides the technical foundation for the proposed G-iMUSIC approaches introduced in Section IV. Throughout this section, we assume that the number of targets K is known. In practice, K can efficiently be estimated with model-order selection methods. The numerical results in Section VII integrate and compare two variants of such strategies.

A. Maximum-Likelihood Estimation

We first formulate the MLE for multi-target DoA estimation. Assuming known (or pre-estimated) noise variance σ^2 , we gather the unknown parameters in $\gamma = [\Theta^T \text{vec}(\mathbf{B}')]^T$. The MLE identifies the estimate $\hat{\gamma}$ that maximizes the likelihood of \mathbf{Y} under the observation model in (7). Because observations are independent across OFDM symbols and subcarriers, the likelihood factorizes into Gaussian terms; after taking the logarithm and removing constants, we obtain

$$\hat{\gamma} = \arg \min_{\tilde{\gamma}} \left\| \mathbf{Y} - \mathbf{A}(\tilde{\Theta}) \tilde{\mathbf{B}}' \right\|_{\text{F}}^2. \quad (10)$$

We next solve (10) with respect to the channel coefficients $\tilde{\mathbf{B}}'$, which gives a closed-form expression as a function of $\tilde{\Theta}$:

$$\tilde{\mathbf{B}}' = \left(\mathbf{A}^\dagger(\tilde{\Theta}) \mathbf{A}(\tilde{\Theta}) \right)^{-1} \mathbf{A}^\dagger(\tilde{\Theta}) \mathbf{Y} = \mathbf{A}^+(\tilde{\Theta}) \mathbf{Y}, \quad (11)$$

where $\mathbf{A}^+(\tilde{\Theta}) = \left(\mathbf{A}^\dagger(\tilde{\Theta}) \mathbf{A}(\tilde{\Theta}) \right)^{-1} \mathbf{A}^\dagger(\tilde{\Theta})$ denotes the Moore-Penrose pseudoinverse [2]. By substituting (11) into (10) and introducing the projection matrix onto the steering-matrix column space, $\mathbf{P}(\tilde{\Theta}) = \mathbf{A}(\tilde{\Theta}) \mathbf{A}^+(\tilde{\Theta})$, we obtain the concentrated log-likelihood problem:

$$\hat{\Theta} = \arg \min_{\tilde{\Theta}} \left\| \mathbf{Y} - \mathbf{P}(\tilde{\Theta}) \mathbf{Y} \right\|_{\text{F}}^2. \quad (12)$$

After algebraic manipulations, this problem reduces to

$$\hat{\Theta} = \arg \max_{\tilde{\Theta}} \left\| \mathbf{Y}^\dagger \mathbf{P}(\tilde{\Theta}) \right\|_{\text{F}}^2, \quad (13)$$

$$= \arg \max_{\tilde{\Theta}} \text{Tr} \left[\mathbf{R} \mathbf{P}(\tilde{\Theta}) \right], \quad (14)$$

$$= \arg \max_{\tilde{\Theta}} \left\| \left(\mathbf{R}^{1/2} \right)^\dagger \mathbf{P}(\tilde{\Theta}) \right\|_{\text{F}}^2. \quad (15)$$

where we define $\mathbf{R} = \frac{1}{DQ} \mathbf{Y} \mathbf{Y}^\dagger \in \mathbb{C}^{M \times M}$ as the sample covariance matrix of the received signal. All three forms in (13), (14), and (15) are equivalent, but the latter is less conventional in the literature. It is presented because it is useful for the developments in Sections III-C and IV. It is expressed in terms of the square-root residual sample covariance matrix $\mathbf{R}^{1/2}$ that can have any size for the column dimension, as long

Algorithm 1: MUSIC and WMUSIC**Input:** K and \mathbf{R} **Output:** $\hat{\Theta} = [\hat{\theta}_1 \dots \hat{\theta}_K]$ **begin**

1. **EVD:** Compute eigenvalues/eigenvectors of \mathbf{R} ;
2. **Signal/Noise partition:** $\mathbf{R} = \mathbf{U}\mathbf{\Lambda}\mathbf{U}^\dagger + \mathbf{G}\mathbf{\Sigma}\mathbf{G}^\dagger$;
3. **Pseudospectrum evaluation:** $\forall \tilde{\theta} \in \mathcal{G}_\theta$,
 - a) MUSIC: $\mathcal{J}_\mathbf{G}(\tilde{\theta})$ in (17) or $\mathcal{J}_\mathbf{U}(\tilde{\theta})$ in (18);
 - b) WMUSIC: $\mathcal{J}_{\Sigma\mathbf{G}}(\tilde{\theta})$ in (19) or $\mathcal{J}_{\Lambda\mathbf{U}}(\tilde{\theta})$ in (20);
4. **Peak selection:** $\hat{\Theta} \leftarrow K$ largest peaks in \mathcal{J} ;

as $\mathbf{R}^{1/2} \mathbf{R}^{1/2\dagger} = \mathbf{R}$ holds. As such, $\mathbf{Y}, \in \mathbb{C}^{M \times DQ}$ is a valid square-root sample covariance matrix. In this work, we use $\mathbf{R}^{1/2} \in \mathbb{C}^{M \times M}$, which is more compact and computationally efficient than \mathbf{Y} as shown in the complexity analysis of Section VI. Such $\mathbf{R}^{1/2}$ form can be obtained via Cholesky decomposition, EVD, or other methods.

The MLE solution is given by the K DoA estimates in $\hat{\Theta}$ that maximize (13) (or equivalently (14) or (15)). In practice, however, exact MLE remains computationally prohibitive, with complexity scaling as $\mathcal{O}(N^K M^3)$, where N is the number of grid points per DoA variable.

B. Subspace Methods: MUSIC and WMUSIC

Because exact MLE is intractable in many scenarios, subspace methods such as MUSIC and WMUSIC are widely used alternatives. They provide super-resolution behavior at substantially lower complexity [15]–[18]. Empirical evidence further indicates that MUSIC often outperforms its weighted counterpart in peak detection [16]. Algorithm 1 summarizes this workflow, which is detailed below.

1) *Eigenvalue Decomposition:* The first step computes the EVD of the sample covariance matrix \mathbf{R} .

2) *Signal- and Noise-Subspace Partition:* We partition \mathbf{R} into signal and noise components using the computed eigenpairs. The dimensionality of the signal subspace is typically set to match the number K of targets. The signal subspace $\mathbf{U} \in \mathbb{C}^{M \times K}$ spans the K dominant eigenvectors, while the noise subspace $\mathbf{G} \in \mathbb{C}^{M \times (M-K)}$ spans the remaining eigenvectors. Hence,

$$\mathbf{R} = \mathbf{U}\mathbf{\Lambda}\mathbf{U}^\dagger + \mathbf{G}\mathbf{\Sigma}\mathbf{G}^\dagger, \quad (16)$$

where the diagonal signal and noise eigenvalue matrices are denoted as $\mathbf{\Lambda}$ and $\mathbf{\Sigma}$, respectively.

3) *Pseudospectrum Evaluation:* The MUSIC pseudospectrum is evaluated over a search grid \mathcal{G}_θ of N candidate DoA values. To reduce complexity, we evaluate either a noise-subspace or a signal-subspace form, depending on the subspace dimensions. When the signal subspace is larger ($K > M - K$), we use $\mathbf{G}\mathbf{G}^\dagger$; otherwise, we use $\mathbf{U}\mathbf{U}^\dagger$. The corresponding pseudo-spectra are

$$\mathcal{J}_\mathbf{G}(\tilde{\theta}) = \frac{1}{\mathbf{a}^\dagger(\tilde{\theta}) \mathbf{G}\mathbf{G}^\dagger \mathbf{a}(\tilde{\theta})} = \left\| \mathbf{G}^\dagger \mathbf{a}(\tilde{\theta}) \right\|_2^{-2}, \quad (17)$$

$$\mathcal{J}_\mathbf{U}(\tilde{\theta}) = \mathbf{a}^\dagger(\tilde{\theta}) \mathbf{U}\mathbf{U}^\dagger \mathbf{a}(\tilde{\theta}) = \left\| \mathbf{U}^\dagger \mathbf{a}(\tilde{\theta}) \right\|_2^2. \quad (18)$$

Algorithm 2: OMP and OLS**Input:** K and \mathbf{Y} or \mathbf{R} **Output:** $\hat{\Theta}_K = [\hat{\theta}_1 \dots \hat{\theta}_K]$ **begin**

1. **Initialization:** $\hat{\Theta}_0 \leftarrow []$, $\mathbf{P}^\perp(\hat{\Theta}_0) \leftarrow \mathbf{I}_M$;
- for** $k \leftarrow 0$ **to** $K - 1$ **do**
 2. **Selection Step:**
 - a) OMP: $\hat{\theta}_{k+1} \leftarrow$ (24) or (25);
 - b) OLS: $\hat{\theta}_{k+1} \leftarrow$ (32) or (33);
 3. **Update Step:**
 $\hat{\Theta}_{k+1} \leftarrow [\hat{\Theta}_k, \hat{\theta}_{k+1}]$, $\mathbf{P}^\perp(\hat{\Theta}_{k+1}) \leftarrow$ (22);

Although $\mathcal{J}_\mathbf{G}$ and $\mathcal{J}_\mathbf{U}$ differ numerically, they share identical peak locations because $\mathbf{U}\mathbf{U}^\dagger + \mathbf{G}\mathbf{G}^\dagger = \mathbf{I}_M$ [16]. For WMUSIC, the pseudo-spectrum is defined similarly but with eigenvalue weighting:

$$\mathcal{J}_{\Sigma\mathbf{G}}(\tilde{\theta}) = \frac{1}{\mathbf{a}^\dagger(\tilde{\theta}) \mathbf{G}\mathbf{\Sigma}\mathbf{G}^\dagger \mathbf{a}(\tilde{\theta})} = \left\| (\mathbf{\Sigma}^{1/2} \mathbf{G})^\dagger \mathbf{a}(\tilde{\theta}) \right\|_2^{-2}, \quad (19)$$

$$\mathcal{J}_{\Lambda\mathbf{U}}(\tilde{\theta}) = \mathbf{a}^\dagger(\tilde{\theta}) \mathbf{U}\mathbf{\Lambda}\mathbf{U}^\dagger \mathbf{a}(\tilde{\theta}) = \left\| (\mathbf{\Lambda}^{1/2} \mathbf{U})^\dagger \mathbf{a}(\tilde{\theta}) \right\|_2^2. \quad (20)$$

Since $\mathbf{\Lambda}$ and $\mathbf{\Sigma}$ are diagonal, their square-root matrices are obtained by taking the square root of each eigenvalue. By contrast to standard MUSIC, the weighted forms $\mathcal{J}_{\Sigma\mathbf{G}}$ and $\mathcal{J}_{\Lambda\mathbf{U}}$ do not necessarily peak at the same locations, because weighting breaks the complementary projection relation in (16). As a result, these two weighted variants may perform differently depending on the scenario.

4) *Peak Selection:* We then identify the K most prominent peaks of the pseudo-spectrum to obtain $\hat{\Theta} = [\hat{\theta}_1 \dots \hat{\theta}_K]$. Optionally, gradient-ascent refinement at each detected peak mitigates grid quantization effects and enables off-grid localization in the continuous domain.

C. Greedy Methods: OMP and OLS

We now move from subspace estimation to greedy methods that approximate MLE at lower cost. Both OMP and OLS estimate targets by selecting one DoA per iteration while leveraging previously selected DoAs. We denote the estimated DoA set at iteration k as $\hat{\Theta}_k = [\hat{\theta}_1 \dots \hat{\theta}_k]$. The projection operators onto the subspace generated by the columns of $\mathbf{A}(\hat{\Theta}_k)$, and onto its orthogonal complement, are defined as

$$\mathbf{P}(\hat{\Theta}_k) = \mathbf{A}(\hat{\Theta}_k) \mathbf{A}^+(\hat{\Theta}_k), \quad (21)$$

$$\mathbf{P}^\perp(\hat{\Theta}_k) = \mathbf{I}_M - \mathbf{P}(\hat{\Theta}_k). \quad (22)$$

Algorithm 2 summarizes the common framework of OMP and OLS, which we detail next.

1) *Initialization:* Both algorithms initialize with an empty DoA set $\hat{\Theta}_0$ and target counter $k = 0$. At initialization, $\mathbf{P}^\perp(\hat{\Theta}_0) = \mathbf{I}_M$, which spans the full observation space. The algorithm then alternates between selection and update steps until K targets are estimated.

2) *Selection Step*: To express the selection criterion, we define the residual observation and covariance matrices as

$$\mathbf{Y}_k = \mathbf{P}^\perp(\widehat{\Theta}_k) \mathbf{Y} \quad \text{and} \quad \mathbf{R}_k = \mathbf{P}^\perp(\widehat{\Theta}_k) \mathbf{R} \mathbf{P}^\perp(\widehat{\Theta}_k). \quad (23)$$

Each iteration selects the next target DoA by solving a one-dimensional optimization problem over \mathcal{G}_θ . Similarly to MUSIC, optional gradient-ascent refinement can be used for off-grid estimation. The OMP and OLS methods differ in the objective function, as detailed below. OMP selects the next target DoA $\widehat{\theta}_{k+1}$ by maximizing the correlation between the steering vector and the residual observation matrix

$$\widehat{\theta}_{k+1}^{\text{OMP}} = \arg \max_{\theta_{k+1}} \left\| \mathbf{Y}_k^\dagger \mathbf{a}(\widetilde{\theta}_{k+1}) \right\|_2^2, \quad (24)$$

$$= \arg \max_{\theta_{k+1}} \mathbf{a}^\dagger(\widetilde{\theta}_{k+1}) \mathbf{R}_k \mathbf{a}(\widetilde{\theta}_{k+1}), \quad (25)$$

$$= \arg \max_{\theta_{k+1}} \left\| (\mathbf{R}_k^{1/2})^\dagger \mathbf{a}(\widetilde{\theta}_{k+1}) \right\|_2^2. \quad (26)$$

Again, all three forms are equivalent, but the last one is less conventional in the literature. It is expressed in terms of the square-root residual sample covariance matrix, defined as

$$\mathbf{R}_k^{1/2} = \mathbf{P}^\perp(\widehat{\Theta}_k) \mathbf{R}^{1/2}, \in \mathbb{C}^{M \times M}. \quad (27)$$

To avoid redundant computations, we compute $\mathbf{R}^{1/2}$ once before the iterations and then reuse it for every update of $\mathbf{R}_k^{1/2}$ from (27). The OMP selection problem is equivalent to solving a univariate MLE problem on the residual observation matrix \mathbf{Y}_k or sample covariance matrix \mathbf{R}_k . By contrast, OLS selects $\widehat{\theta}_{k+1}$ by minimizing the least-squares error at each iteration:

$$\widehat{\theta}_{k+1}^{\text{OLS}} = \arg \max_{\theta_{k+1}} \left\| \mathbf{Y}_k^\dagger \mathbf{P}([\widehat{\Theta}_k, \widetilde{\theta}_{k+1}]) \right\|_{\text{F}}^2, \quad (28)$$

$$= \arg \max_{\theta_{k+1}} \text{Tr} \left[\mathbf{R} \mathbf{P}([\widehat{\Theta}_k, \widetilde{\theta}_{k+1}]) \right], \quad (29)$$

$$= \arg \max_{\theta_{k+1}} \left\| (\mathbf{R}_k^{1/2})^\dagger \mathbf{P}([\widehat{\Theta}_k, \widetilde{\theta}_{k+1}]) \right\|_{\text{F}}^2. \quad (30)$$

These formulations are equivalent to a $(k+1)$ -dimensional MLE constrained by the previously selected set $\widehat{\Theta}_k$, so that only the candidate DoA $\widetilde{\theta}_{k+1}$ is searched over one dimension. Intuitively, OLS jointly reoptimizes the candidate DoA and the modulated channel coefficients of all previously selected DoAs plus the candidate, whereas OMP optimizes only the candidate DoA and its corresponding coefficient. This joint optimization improves estimation accuracy but drastically increases computational complexity. To alleviate this burden, previous works [13], [25] have leveraged a projection-matrix decomposition demonstrating that

$$\mathbf{P}([\widehat{\Theta}_k, \widetilde{\theta}_{k+1}]) = \mathbf{P}(\widehat{\Theta}_k) + \frac{\mathbf{a}_k(\widetilde{\theta}_{k+1}) \mathbf{a}_k^\dagger(\widetilde{\theta}_{k+1})}{\|\mathbf{a}_k(\widetilde{\theta}_{k+1})\|_2^2}, \quad (31)$$

where $\mathbf{a}_k(\widetilde{\theta}_{k+1}) = \mathbf{P}^\perp(\widehat{\Theta}_k) \mathbf{a}(\widetilde{\theta}_{k+1})$. By substituting (31) into (28), (29), and (30), and then removing terms independent of $\widetilde{\theta}_{k+1}$, we obtain the following efficient forms

$$\widehat{\theta}_{k+1}^{\text{OLS}} = \arg \max_{\theta_{k+1}} \frac{\|\mathbf{Y}_k^\dagger \mathbf{a}(\widetilde{\theta}_{k+1})\|_2^2}{\|\mathbf{a}_k(\widetilde{\theta}_{k+1})\|_2^2}, \quad (32)$$

$$= \arg \max_{\theta_{k+1}} \frac{\mathbf{a}^\dagger(\widetilde{\theta}_{k+1}) \mathbf{R}_k \mathbf{a}(\widetilde{\theta}_{k+1})}{\|\mathbf{a}_k(\widetilde{\theta}_{k+1})\|_2^2}, \quad (33)$$

$$= \arg \max_{\theta_{k+1}} \frac{\|(\mathbf{R}_k^{1/2})^\dagger \mathbf{a}(\widetilde{\theta}_{k+1})\|_2^2}{\|\mathbf{a}_k(\widetilde{\theta}_{k+1})\|_2^2}. \quad (34)$$

The denominator captures the projection of the steering vector onto the orthogonal complement of previously selected angles, thereby normalizing the OMP-like numerator.

3) *Update Step*: After each selection, we update the angle set and the orthogonal-complement projection matrix to include the newly estimated angle $\widehat{\theta}_{k+1}$. This update defines the residual observation space used in the next iteration.

IV. GREEDY ITERATIVE MUSIC ALGORITHMS

This section introduces the proposed G-iMUSIC algorithms for multi-target DoA estimation. These algorithms integrate MUSIC-based subspace pseudo-spectrum evaluations into the greedy OMP and OLS frameworks to improve and accelerate target-DoA selection. As in Section III, we assume that the number of targets K is known; the discussion about practical model-order selection is deferred to Section VII.

We first present a unified framework that links subspace estimation and greedy optimization, thereby motivating the proposed algorithms. We then detail the processing steps of OMP-iMUSIC and OLS-iMUSIC, along with their weighted iMUSIC variants.

A. Unified Subspace and Greedy Estimation Framework

This link relies on reformulating the OMP and OLS selection steps using a MUSIC-like signal-noise subspaces decomposition of $\mathbf{R}_k^{1/2}$. The resulting expressions are stated in Lemma 1, in which the residual signal and noise subspace matrices at iteration k are defined as

$$\mathbf{U}_k = \mathbf{P}^\perp(\Theta_k) \mathbf{U}, \quad \mathbf{G}_k = \mathbf{P}^\perp(\Theta_k) \mathbf{G}. \quad (35)$$

Lemma 1. *The OMP and OLS selection steps in (26) and (34) can be equivalently expressed as a function of the residual signal and noise subspaces as*

$$\widehat{\theta}_{k+1}^{\text{OMP}} = \arg \max_{\theta_{k+1}} \left\| (\mathbf{U}_k \mathbf{\Lambda}^{1/2} + \mathbf{G}_k \mathbf{\Sigma}^{1/2})^\dagger \mathbf{a}(\widetilde{\theta}_{k+1}) \right\|_2^2, \quad (36)$$

$$\widehat{\theta}_{k+1}^{\text{OLS}} = \arg \max_{\theta_{k+1}} \frac{\left\| (\mathbf{U}_k \mathbf{\Lambda}^{1/2} + \mathbf{G}_k \mathbf{\Sigma}^{1/2})^\dagger \mathbf{a}(\widetilde{\theta}_{k+1}) \right\|_2^2}{\|\mathbf{a}_k(\widetilde{\theta}_{k+1})\|_2^2}. \quad (37)$$

Proof. From (16) and because the signal and noise subspaces are orthogonal, $\mathbf{R}^{1/2} = \mathbf{U} \mathbf{\Lambda}^{1/2} + \mathbf{G} \mathbf{\Sigma}^{1/2}$. \square

Building on Lemma 1, we approximate the common expressions of the OMP objective function in (36) and of the

numerator of the OLS objective function in (37) through a low-rank argument as follows

$$\begin{aligned} & \|(\mathbf{U}_k \mathbf{\Lambda}^{1/2} + \mathbf{G}_k \mathbf{\Sigma}^{1/2})^\dagger \mathbf{a}(\tilde{\theta}_{k+1})\|_2^2 \\ & \stackrel{(a)}{=} \|(\mathbf{U}_k \mathbf{\Lambda}^{1/2})^\dagger \mathbf{a}(\tilde{\theta}_{k+1})\|_2^2 + \|(\mathbf{G}_k \mathbf{\Sigma}^{1/2})^\dagger \mathbf{a}(\tilde{\theta}_{k+1})\|_2^2, \\ & \stackrel{(b)}{\approx} \|(\mathbf{U}_k \mathbf{\Lambda}^{1/2})^\dagger \mathbf{a}(\tilde{\theta}_{k+1})\|_2^2 + 0. \end{aligned} \quad (38)$$

Step (a) follows from the orthogonality of the signal and noise subspaces, which cancels the cross terms when the norm in (36) is expanded, and step (b) neglects the noise-subspace term. This is justified because noise-subspace eigenvalues are typically much smaller than signal-subspace eigenvalues and because target steering vectors have near-zero projection onto the noise subspace. Consequently, evaluating the resulting expression in (38) for all candidate DoA at each step k corresponds to a WMUSIC pseudospectrum evaluation, as in (20), but based on the residual signal subspace.

B. Proposed G-iMUSIC Selection Step

From this derivation, we can define two weighted variants of the proposed G-iMUSIC algorithms, which we refer to as OMP-iWMUSIC and OLS-iWMUSIC, by applying the low-rank approximation in (38) to the objective functions of OMP and OLS in (36) and (37).

These algorithms can be interpreted as greedy methods that, at each iteration, use a WMUSIC pseudospectrum evaluation based on the residual signal subspace to select the next target DoA. Their resulting selection rules are stated in Proposition 1, while their practical implementation steps are detailed in Section IV-C.

Proposition 1. *The OMP-iWMUSIC and OLS-iWMUSIC selection steps are respectively given by*

$$\hat{\theta}_{k+1}^{\text{OMP-iWMUSIC}} = \arg \max_{\theta_{k+1}} \|(\mathbf{U}_k \mathbf{\Lambda}^{1/2})^\dagger \mathbf{a}(\tilde{\theta}_{k+1})\|_2^2, \quad (39)$$

$$\hat{\theta}_{k+1}^{\text{OLS-iWMUSIC}} = \arg \max_{\theta_{k+1}} \frac{\|(\mathbf{U}_k \mathbf{\Lambda}^{1/2})^\dagger \mathbf{a}(\tilde{\theta}_{k+1})\|_2^2}{\|\mathbf{a}_k(\tilde{\theta}_{k+1})\|_2^2}. \quad (40)$$

These selection steps can also be expressed in the residual noise-subspace form as in (19). However, as discussed for WMUSIC, the signal-subspace and noise-subspace forms are not equivalent.

In contrast, empirical evidence suggests that unweighted MUSIC often outperforms its weighted counterpart [16]. Motivated by this observation, we further simplify (38) as follows

$$\|(\mathbf{U}_k \mathbf{\Lambda}^{1/2})^\dagger \mathbf{a}(\tilde{\theta}_{k+1})\|_2^2 \stackrel{(c)}{\approx} \|\mathbf{U}_k^\dagger \mathbf{a}(\tilde{\theta}_{k+1})\|_2^2, \quad (41)$$

$$\stackrel{(d)}{=} \|\mathbf{a}_k(\tilde{\theta}_{k+1})\|_2^2 - \|\mathbf{G}_k^\dagger \mathbf{a}(\tilde{\theta}_{k+1})\|_2^2. \quad (42)$$

Step (c) removes the signal-eigenvalue weighting, and step (d) rewrites the resulting expression in terms of the residual noise subspace by applying $\mathbf{U}_k \mathbf{U}_k^\dagger = \mathbf{P}^\perp(\Theta_k) - \mathbf{G}_k \mathbf{G}_k^\dagger$, and then expanding the norm. Observe now that evaluating the resulting expression in (41) for all candidate DoA, at each step k , corresponds to a MUSIC pseudospectrum evaluation, as in (20), but based on the residual signal subspace. Similarly, the

second term in (42) corresponds to a MUSIC pseudospectrum evaluation based on the residual noise subspace, as in (19).

Consequently, we can define two additional variants of the proposed G-iMUSIC algorithms, which we refer to as OMP-iMUSIC and OLS-iMUSIC, by applying the unweighted low-rank approximation in (41) or (42).

These algorithms can be interpreted as greedy methods that, at each iteration, use a MUSIC pseudospectrum evaluation based on either the residual signal or noise subspace to select the next target DoA. Their resulting selection rules are stated in Proposition 2, while their practical implementation steps are detailed next.

Proposition 2. *The OMP-iMUSIC and OLS-iMUSIC selection steps based on the residual signal and noise subspace are respectively defined as*

$$\hat{\theta}_{k+1}^{\text{OMP-iMUSIC}} = \arg \max_{\tilde{\theta}_{k+1}} \|\mathbf{U}_k^\dagger \mathbf{a}(\tilde{\theta}_{k+1})\|_2^2, \quad (43)$$

$$= \arg \max_{\tilde{\theta}_{k+1}} \|\mathbf{a}_k(\tilde{\theta}_{k+1})\|_2^2 - \|\mathbf{G}_k^\dagger \mathbf{a}(\tilde{\theta}_{k+1})\|_2^2, \quad (44)$$

$$\hat{\theta}_{k+1}^{\text{OLS-iMUSIC}} = \arg \max_{\tilde{\theta}_{k+1}} \frac{\|\mathbf{U}_k^\dagger \mathbf{a}(\tilde{\theta}_{k+1})\|_2^2}{\|\mathbf{a}_k(\tilde{\theta}_{k+1})\|_2^2}, \quad (45)$$

$$= \arg \max_{\tilde{\theta}_{k+1}} 1 - \frac{\|\mathbf{G}_k^\dagger \mathbf{a}(\tilde{\theta}_{k+1})\|_2^2}{\|\mathbf{a}_k(\tilde{\theta}_{k+1})\|_2^2}. \quad (46)$$

The signal and noise subspace forms are equivalent in the sense that they yield the same selection result. However, the noise-subspace form in (44) is less attractive in practice because it introduces an additional operation for the first term compared with (43).

In conclusion, the proposed OMP-iMUSIC and OLS-iMUSIC selection steps in (43) and (44) are a direct application of the MUSIC and WMUSIC pseudospectrum evaluation based on the residual signal subspace, respectively in (18) and (20). The OLS variants in (45) and (46) are a modified versions of the same criteria, as they include an additional normalization term in the denominator, which improves the estimation performance at the price of an additional computation.

C. Practical G-iMUSIC Implementation

Algorithm 3 summarizes the successive steps of the proposed G-iMUSIC methods for multi-target DoA estimation. To clarify this workflow, the following subsections detail each processing step.

1) *Eigenvalue Decomposition:* The first step computes the EVD of the sample covariance matrix \mathbf{R} . Unlike prior iMUSIC approaches that require an EVD at each iteration, the proposed algorithms perform only one EVD at initialization to obtain the signal and noise subspaces. Then, the residual subspaces are updated at each iteration through simple matrix multiplications with the projection matrix $\mathbf{P}^\perp(\Theta_k)$, as in (35).

2) *Signal- and Noise-Subspace Partition:* Using the computed eigenpairs, we next partition \mathbf{R} into signal and noise components, as in Section III-B2.

Algorithm 3: The proposed G-iMUSIC algorithms**Input:** K and \mathbf{Y} or \mathbf{R} **Output:** $\hat{\Theta}_K = [\hat{\theta}_1 \dots \hat{\theta}_K]$ **begin**

1. **EVD:** Compute eigenvalues/eigenvectors of \mathbf{R} ;
2. **Signal/Noise partition:** $\mathbf{R} = \mathbf{U}\mathbf{A}\mathbf{U}^\dagger + \mathbf{G}\mathbf{\Sigma}\mathbf{G}^\dagger$;
3. **Initialization:** $\hat{\Theta}_0 \leftarrow []$, $\mathbf{P}^\perp(\hat{\Theta}_0) \leftarrow \mathbf{I}_M$ and $\mathbf{U}_0 \leftarrow \mathbf{U}$ or $\mathbf{G}_0 \leftarrow \mathbf{G}$;
- for** $k \leftarrow 0$ **to** $K - 1$ **do**
 4. **Selection Step:**
 - a) OMP-iWMUSIC: $\hat{\theta}_{k+1} \leftarrow (39)$;
 - b) OLS-iWMUSIC: $\hat{\theta}_{k+1} \leftarrow (40)$;
 - c) OMP-iMUSIC: $\hat{\theta}_{k+1} \leftarrow (43)$;
 - d) OLS-iMUSIC: $\hat{\theta}_{k+1} \leftarrow (45)$ or (46) ;
 5. **Update Step:** $\hat{\Theta}_{k+1} \leftarrow [\hat{\Theta}_k, \hat{\theta}_{k+1}]$, $\mathbf{P}^\perp(\hat{\Theta}_{k+1}) \leftarrow (22)$ and $\mathbf{U}_k \leftarrow \mathbf{P}^\perp(\hat{\Theta}_k) \mathbf{U}$ or $\mathbf{G}_k \leftarrow \mathbf{P}^\perp(\hat{\Theta}_k) \mathbf{G}$;

3) *Initialization:* Initialization follows the standard greedy methods procedure detailed in Section III-C. Depending on the selected criterion, we additionally initialize one residual subspace matrix, i.e., $\mathbf{U}_0 = \mathbf{U}$ or $\mathbf{G}_0 = \mathbf{G}$. The algorithm then alternates between selection and update steps until all targets are estimated.

4) *Selection Step:* At each iteration, the algorithm selects the next target DoA by solving an optimization problem over the search grid \mathcal{G}_θ . Optionally, gradient ascent refinement can enable off-grid target detection. Depending on the variant of interest, the selection step uses the criteria defined in Proposition 2 or Proposition 1.

5) *Update Step:* After selection, the update step is described in Section III-C. In parallel, we update the residual signal or noise subspace matrices at each iteration from (35).

V. FAST FOURIER TRANSFORM ACCELERATION

This section presents FFT-based accelerations for the algorithms introduced in Sections III and IV in the ULA setting.

For each algorithm, the selection step evaluates an objective function over a grid \mathcal{G}_θ of candidate DoA values. We denote by $\mathbf{J} \in \mathbb{R}^{1 \times N}$ the vector containing these evaluations for all N grid points. In general, \mathbf{J} is obtained by replacing the steering vector $\mathbf{a}(\theta_n)$ in the corresponding objective function with the steering matrix $\mathbf{A}(\mathcal{G}_\theta)$ and then applying the column-wise ℓ_2 norm $\|\cdot\|_{2,c}$. When the array is a ULA, $\mathbf{A}(\mathcal{G}_\theta)$ admits a Discrete Fourier Transform (DFT) representation, which can be computed efficiently using the FFT. Accordingly, we define the DFT matrix $\mathbf{F} \in \mathbb{C}^{M \times N}$ with entries $f_{m,n} = e^{-j2\pi mn/N}$ for antenna indices $m = 0, \dots, M - 1$ and normalized frequency indices $n = 0, \dots, N - 1$. These normalized frequencies are then mapped to their corresponding DoA values in \mathcal{G}_θ .

With this notation in place, the MUSIC (respectively, WMUSIC) pseudospectrum evaluations based on the noise

subspace in (17) (respectively, (19)) and on the signal subspace in (18) (respectively, (20)) can be written equivalently as

$$\mathbf{J}_{\mathbf{G}}^{\text{MUSIC}} = \|\mathbf{G}^\dagger \mathbf{F}\|_{2,c}^{-2}, \quad \mathbf{J}_{\Sigma\mathbf{G}}^{\text{WMUSIC}} = \left\| (\Sigma^{1/2} \mathbf{G})^\dagger \mathbf{F} \right\|_{2,c}^{-2}, \quad (47)$$

$$\mathbf{J}_{\mathbf{U}}^{\text{MUSIC}} = \|\mathbf{U}^\dagger \mathbf{F}\|_{2,c}^2, \quad \mathbf{J}_{\Lambda\mathbf{U}}^{\text{WMUSIC}} = \left\| (\Lambda^{1/2} \mathbf{U})^\dagger \mathbf{F} \right\|_{2,c}^2. \quad (48)$$

Similarly, at each iteration k , the OMP objective values over the grid can be computed from the residual observation matrix \mathbf{Y}_k in (24) and from the residual sample covariance matrix \mathbf{R}_k in (26) as

$$\mathbf{J}_{\mathbf{Y}_k}^{\text{OMP}} = \|\mathbf{Y}_k^\dagger \mathbf{F}\|_{2,c}^2, \quad \mathbf{J}_{\mathbf{R}_k}^{\text{OMP}} = \|(\mathbf{R}_k^{1/2})^\dagger \mathbf{F}\|_{2,c}^2. \quad (49)$$

For MUSIC and OMP, such FFT-based accelerations are already known in the literature. For OLS, in contrast, a DFT formulation of the objective function is available only by exploiting the projection-matrix decomposition in [13], [25]. Building on that decomposition, Proposition 3 provides an FFT-based acceleration of OLS.

Proposition 3. *In the case of ULAs, the evaluation of the OLS objective functions in (32) and (34) can be accelerated through the following element-wise FFT quotients, respectively:*

$$\mathbf{J}_{\mathbf{Y}_k}^{\text{OLS}} = \frac{\|\mathbf{Y}_k^\dagger \mathbf{F}\|_{2,c}^2}{\|\mathbf{P}^\perp(\hat{\Theta}_k) \mathbf{F}\|_{2,c}^2}, \quad \mathbf{J}_{\mathbf{R}_k}^{\text{OLS}} = \frac{\|(\mathbf{R}_k^{1/2})^\dagger \mathbf{F}\|_{2,c}^2}{\|\mathbf{P}^\perp(\hat{\Theta}_k) \mathbf{F}\|_{2,c}^2}. \quad (50)$$

Having established the OLS case, we now turn to the proposed G-iMUSIC methods. Proposition 4 presents the FFT-based accelerations of OMP-iMUSIC and OLS-iMUSIC.

Proposition 4. *In the case of ULAs, the computation of the OMP-iMUSIC objective function in (43) can be accelerated using an FFT as*

$$\mathbf{J}_{\mathbf{U}_k}^{\text{OMP-iMUSIC}} = \|\mathbf{U}_k^\dagger \mathbf{F}\|_{2,c}^2. \quad (51)$$

The evaluation of the OLS-iMUSIC objective functions in (45) and (46) can be accelerated through the following element-wise FFT quotients, respectively:

$$\mathbf{J}_{\mathbf{U}_k}^{\text{OLS-iMUSIC}} = \frac{\|\mathbf{U}_k^\dagger \mathbf{F}\|_{2,c}^2}{\|\mathbf{P}^\perp(\hat{\Theta}_k) \mathbf{F}\|_{2,c}^2}, \quad (52)$$

$$\mathbf{J}_{\mathbf{G}_k}^{\text{OLS-iMUSIC}} = 1 - \frac{\|\mathbf{G}_k^\dagger \mathbf{F}\|_{2,c}^2}{\|\mathbf{P}^\perp(\hat{\Theta}_k) \mathbf{F}\|_{2,c}^2}. \quad (53)$$

By the same argument, weighted variants are accelerated by replacing the signal and noise subspace matrices with their weighted counterparts, as in WMUSIC.

VI. COMPUTATIONAL COMPLEXITY ANALYSIS

In this section, we present the asymptotic computational complexity of the algorithms presented in Sections III and IV. Table II summarizes the number of floating-point operations (FLOPs) for the main processing steps of each algorithm. Unless stated otherwise, these counts are expressed as a function of key system parameters by following standard FLOP models for basic matrix operations [26], [27]. The number of flops in

TABLE II

THEORETICAL COMPLEXITY COMPARISON OF THE MAIN PROCESSING STEPS OF THE CONSIDERED MULTI-TARGET DOA ESTIMATION METHODS WITHOUT FFT ACCELERATION. IN CASE OF A ULA, THE FFT ACCELERATION REDUCES THE COMPLEXITY OF THE OBJECTIVE FUNCTION EVALUATION BY REPLACING NM BY $N \log_2(M)$. FOR CONCISENESS, WE DEFINE $K_M = \min(K, M - K)$.

	MUSIC	OMP-Y	OLS-Y	OMP-R ^{1/2}	OLS-R ^{1/2}	OMP-iMUSIC	OLS-iMUSIC
$\mathbf{R} = \frac{1}{DQ} \mathbf{Y} \mathbf{Y}^\dagger$	$\mathcal{O}(DQM^2)$	-	-	$\mathcal{O}(DQM^2)$	$\mathcal{O}(DQM^2)$	$\mathcal{O}(DQM^2)$	$\mathcal{O}(DQM^2)$
EVD of \mathbf{R}	$\mathcal{O}(M^3)$	-	-	-	-	$\mathcal{O}(M^3)$	$\mathcal{O}(M^3)$
Numerator of objective function	$\mathcal{O}(NMK_M)$	$K \mathcal{O}(NMDQ)$	$K \mathcal{O}(NMDQ)$	$K \mathcal{O}(NM^2)$	$K \mathcal{O}(NM^2)$	$K \mathcal{O}(NMK)$	$K \mathcal{O}(NMK_M)$
Denominator of objective function	-	-	$K \mathcal{O}(NM^2)$	-	$K \mathcal{O}(NM^2)$	-	$K \mathcal{O}(NM^2)$
Peaks detection	$\mathcal{O}(N)$	-	-	-	-	-	-

Table II is provided without the FFT acceleration; its benefit is detailed next.

Assuming each method takes the observation matrix \mathbf{Y} as input, computing the sample covariance matrix \mathbf{R} requires $\mathcal{O}(DQM^2)$ operations. For MUSIC-based methods, computing the EVD of \mathbf{R} requires $\mathcal{O}(M^3)$ FLOPs with standard routines (e.g., the QZ algorithm) [28]. In addition, to exploit FFT acceleration in OMP/OLS methods based on \mathbf{R} , one initial square-root matrix computation is required (for instance via EVD). We next detail the complexity of the selection step for each algorithm. Among the considered methods, MUSIC is the only non-iterative one; hence, it requires a single pseudo-spectrum evaluation over the full grid. As shown in Section III-C, the numerators of the OMP and OLS selection steps are equivalent. However, OLS includes an additional denominator term. For G-iMUSIC-based algorithms, OLS-iMUSIC can evaluate its numerator in either the signal or the noise subspace (Proposition 2), which leads to different complexity expressions. When a ULA is used, all methods can exploit FFT acceleration for numerator and denominator evaluations. This reduces the NM factor to $N \log(M)$ [29]. Finally, because MUSIC detects all targets in one stage, it requires pseudo-spectrum peak detection. This adds $\mathcal{O}(N)$ operations, whereas greedy methods only require maximum-value selection at each iteration. Note that the weighting of the WMUSIC variants is not displayed in Table II, but they do not change the asymptotic complexity of the selection step compared with their unweighted counterparts.

Overall, MUSIC is expected to have the lowest computational complexity as it does not require iterative processing. However, it requires a peak-detection step that greedy methods do not require. Traditional OMP algorithms exhibit lower complexity than OLS due to the absence of a denominator term, although this gap is substantially reduced compared with naive OLS implementations thanks to the projection-matrix decomposition in (31). The implementation based on $\mathbf{R}^{1/2}$ is usually preferred over the one based on \mathbf{Y} because $DQ \gg M$ in the considered scenario. Moreover, the presented G-iMUSIC algorithms have lower complexity than their traditional OMP and OLS counterparts as they project steering vectors onto either the residual signal or noise subspaces rather than $\mathbf{R}_k^{1/2}$. Thanks to the possible evaluation of the OLS-

iMUSIC numerator using either the signal or noise subspace, its additional computational burden with respect to OMP-iMUSIC can be reduced, depending on the relative sizes of K and M . Finally, FFT acceleration further reduces the computational burden of all algorithms in ULA configurations. While the asymptotic analysis in Table II identifies the dominant computational components of each method, it does not fully capture practical runtime behavior. Therefore, Section VII complements this analysis with processing-time evaluations.

VII. SIMULATION SETUP AND RESULTS

In this section, we compare the proposed G-iMUSIC algorithms with MUSIC, OMP, and OLS for multi-target DoA estimation in a PR system.

A. Simulation Scenario

We evaluate performance over 10,000 Monte Carlo simulations in a scenario with a colocated AP and PR. In each simulation, we consider a fixed setup in which multiple targets are randomly positioned within a maximum range of $\tau_{max} = 60$ m. We assume half-wavelength antenna spacing and optimal orientation toward the coverage area. Following the Wi-Fi 7 standard, we set the carrier frequency to $f_c = 5$ GHz, and the subcarrier spacing to $\Delta_f = 78.125$ kHz [30]. Unless stated otherwise, the system parameters are $K = 8$ targets, $M = 16$ antennas, $Q = 512$ subcarriers (i.e., 40 MHz), $D = 10$ successive symbols, and an SNR of 40 dB. We compute the mean SNR by averaging (6) across all simulations. With this definition, the SNR is dominated by the strongest target, which is also the easiest to detect. As a result, the radar operating SNR regime may appear higher than that of a conventional communication system. We define a search grid \mathcal{G}_θ with $N = 2048$ uniformly spaced points between -1 and 1 , representing the normalized angular domain.

B. Estimation of the number of targets

In the previous sections, the number of targets K is assumed to be known. In practice, however, this quantity is unknown and must be estimated from the observed data. Target-number estimation can be formulated as a model-order selection problem, which is typically addressed using information theoretic

criteria (ITC). These criteria minimize an objective function that balances a likelihood term against a complexity penalty. In this work, we consider the Akaike information criterion (AIC) criterion of Wax and Kailath [31]. Intuitively, this criterion evaluates the number of targets by assessing the rank of the signal subspace, which is determined by the number of dominant eigenvalues of the sample covariance matrix \mathbf{R} . This rank-based criterion is widely used in the DoA estimation literature and is independent of the specific estimation algorithm from Section III and IV, making it suitable for a fair comparison. In this disjoint approach, the number of targets \hat{K}_{Rank} is first estimated before applying the DoA estimation algorithm. In our previous work [32], we proposed a hybrid criterion that combines the eigenvalue-based AIC of Wax and Kailath [31] with a selection-based criterion that depends on detected OLS peaks. Specifically, the first \hat{K}_{Rank} estimated angles are systematically added to the set of detected peaks $\hat{\Theta}$. Then, the hybrid criterion stops adding new angles when it does not improve the proposed AIC-OLS criterion, yielding $\hat{K}_{\text{Hybrid}} \geq \hat{K}_{\text{Rank}}$ detected targets. This hybrid approach significantly improves OLS and OLS-iMUSIC, but it does not provide a significant gain for MUSIC, OMP, or OMP-iMUSIC. Accordingly, for the two OLS variants, we also report results obtained with the hybrid criterion.

C. Diagnostic Metrics

To interpret the observed performance trends beyond the considered scenario, we introduce two scenario-agnostic diagnostic metrics: the *steering-vector correlation metric* (\mathcal{T}) and the *signal correlation metric* (\mathcal{S}). Together, these metrics provide a compact measure of the difficulty of the detection scenario.

The steering-vector correlation metric \mathcal{T} quantifies the mean angular proximity between targets, which captures the physical resolution of the system. The signal correlation metric \mathcal{S} quantifies the mean correlation between target signals, which can be influenced by their intrinsic correlation or by their temporal and spectral diversity. In the considered passive OFDM radar scenario, the target signals are correlated because they share the same unknown data symbols, but they become less correlated as Q and D increase as the corresponding range and Doppler resolutions improve.

To define these metrics, we introduce the steering-vector resolution matrix $\mathbf{T} \in \mathbb{C}^{K \times K}$ and the signal correlation matrix $\mathbf{S} \in \mathbb{C}^{K \times K}$, which are defined as the normalized Gram matrices of the steering vectors and of the target signals, respectively,

$$\mathbf{T} = \frac{1}{M} \mathbf{A}^\dagger(\Theta) \mathbf{A}(\Theta), \quad \text{and} \quad \mathbf{S} = \frac{1}{DQ} \mathbf{B}' \mathbf{B}'^\dagger. \quad (54)$$

The closer these matrices are to diagonal, the lower the inter-target correlations and, consequently, the more favorable the detection scenario. Their diagonality can be quantified using the criterion proposed in [33], which evaluates the mean ratio between diagonal and off-diagonal entries of a matrix, yielding a score between 0 (for a balanced matrix) and 1 (for a perfectly diagonal matrix). The proposed diagnostic metrics \mathcal{T} and \mathcal{S} are

therefore computed as the average diagonality ratings across the Monte Carlo simulations.

In theory, both \mathcal{T} and \mathcal{S} should correlate positively with detection performance. More specifically, greedy methods such as OMP and OLS are expected to perform better when \mathcal{T} is high, because they rely on the correlation between the residual and the steering vectors to select new peaks. When \mathcal{S} is low, greedy methods become sensitive to early selection errors due to unresolved targets [6]. By contrast, subspace methods such as MUSIC are expected to perform better when \mathcal{S} is high, because their super-resolution capability relies on the separability of the targets in the domains averaged in the sample covariance matrix computation, which are here the time and frequency domains [1].

D. Performance Analysis

The next subsections analyze detection, precision, and timing performance. For the metric evaluations, we associate detected DoAs with true DoAs using the Hungarian algorithm [34]. We count a hit when a detected peak lies within the main lobe of its associated true target DoA. We declare a false alarm when a detected peak cannot be associated with any true target DoA. For visual clarity, we omit the curves of OMP-iWMUSIC and OLS-iWMUSIC in the performance analysis. Their performance is briefly discussed at the end of this section.

1) Detection Performance: We evaluate each algorithm's ability to detect targets using the Youden J statistic, defined as the difference between hit rate and false alarm rate [35], [36]. A score of 1 indicates perfect detection, whereas a score of 0 indicates equal hit and false alarm rates. Fig. 1 reports the Youden J statistic versus SNR, the number of targets K , and the number of subcarriers Q . Because Δ_f is fixed, increasing Q also increases the bandwidth B .

We first examine the SNR sweep in Fig. 1a. At low SNR, greedy methods outperform MUSIC. As the SNR increases, MUSIC approaches greedy methods because signal and noise subspaces become easier to separate. Accordingly, the performance gap between G-iMUSIC and their OMP/OLS counterparts is larger at high SNR.

We next vary the number of targets in Fig. 1b. Detection performance decreases as K increases, as expected to follow the simultaneous decrease of \mathcal{S} and \mathcal{T} . At low K , all methods show similar detection performance. As K increases, however, the gain of OLS-based variants with the hybrid criterion becomes more pronounced. For visual clarity, we omit the hybrid-criterion curves of OMP and OMP-iMUSIC. Although they exceed their eigenvalue-based counterparts at high K , they remain below OLS and OLS-iMUSIC.

Fig. 1c analyzes the effect of Q for both stopping criteria. At low Q , the eigenvalue-based criterion degrades all methods [32]; therefore, we discuss this low- \mathcal{S} regime through the hybrid target selection criterion. As expected, MUSIC fails in this regime. In contrast, the proposed G-iMUSIC variants outperform their OMP/OLS counterparts, indicating stronger robustness for low- \mathcal{S} than MUSIC. As Q increases, methods that rely on the eigenvalue-based AIC criterion improve markedly.

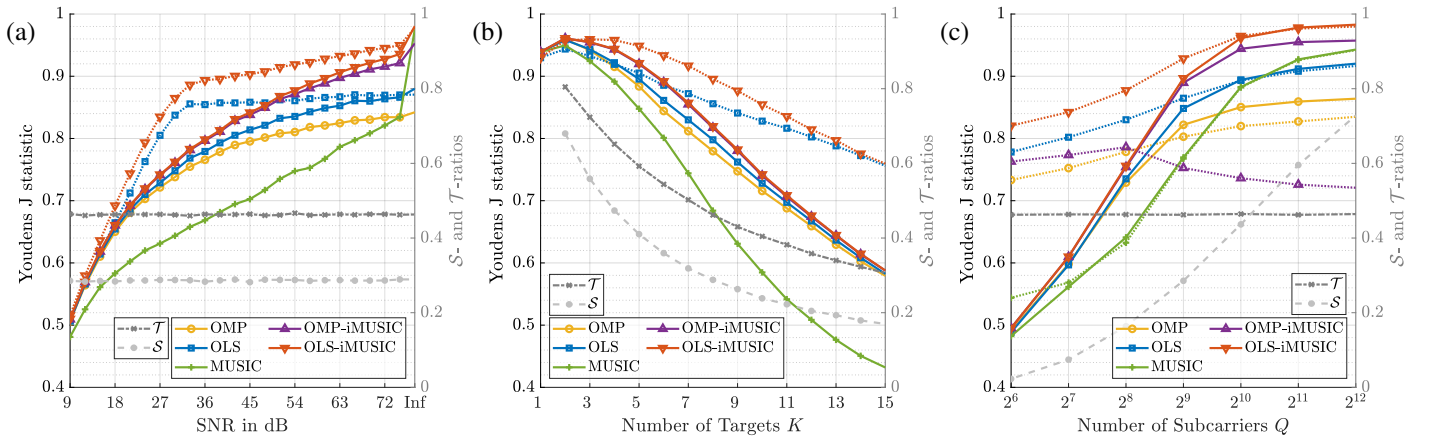


Fig. 1. Youden J statistic versus (a) SNR, (b) number of targets K , and (c) number of subcarriers Q . Solid lines use the eigenvalue-based AIC stopping criterion, whereas dotted lines use the hybrid criterion. In (c), hybrid criterion curves are shown for all methods. The S and T diagnostics are also plotted (dashed light gray and dash-dotted dark gray, respectively).

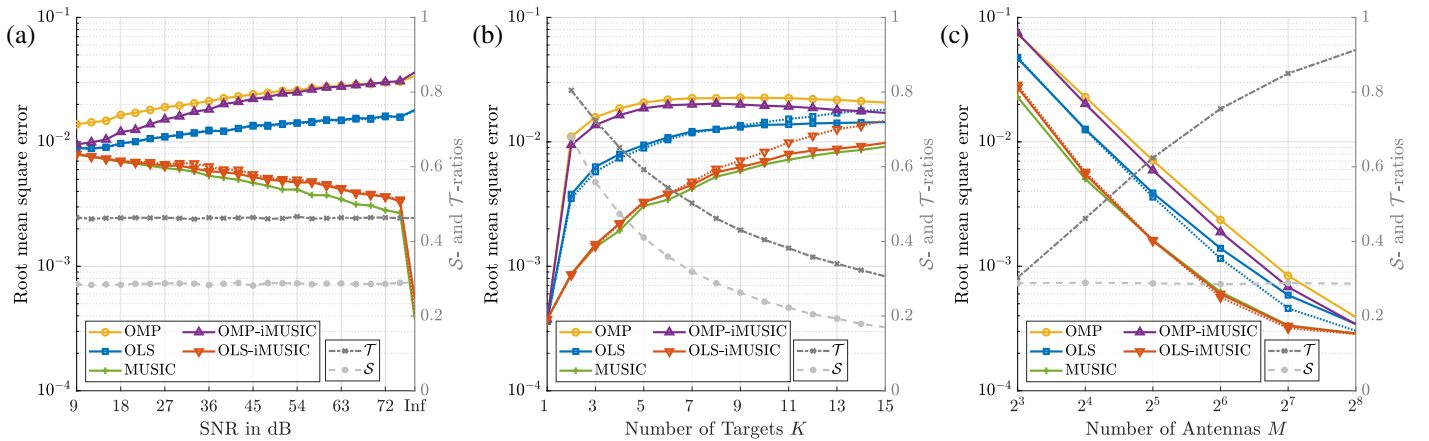


Fig. 2. RMSE versus (a) SNR, (b) number of targets K , and (c) number of antennas M . Solid lines use the eigenvalue-based AIC stopping criterion, whereas dotted lines use the hybrid criterion. The S and T diagnostics are also plotted (dashed light gray and dash-dotted dark gray, respectively).

At high S , OMP-iMUSIC approaches OLS-iMUSIC, which is consistent with the strong behavior of MUSIC in this regime.

Overall, the G-iMUSIC methods consistently outperform their respective OMP and OLS baselines and also outperform MUSIC. Consistent with [32], the hybrid AIC criterion improves both OLS methods compared to the eigenvalue-based AIC criterion. Moreover, the gain of OLS-iMUSIC over OMP-iMUSIC is most visible with the hybrid criterion.

2) Precision Performance: We now turn to precision and evaluate it through the RMSE between true normalized DoAs and estimated normalized DoAs. To ensure a fair comparison, we compute RMSE only on targets that are hits for all methods. In other words, we evaluate precision only on the subset of targets that are detected by all methods, which are typically the easiest ones. Thus, the precision analysis in Figure 2 focuses on the accuracy of peak localization, rather than on the ability to detect difficult targets.

Similarly to the detection analysis, Fig. 2a shows that precision improves with SNR for MUSIC and OLS-iMUSIC. By contrast, for the remaining methods, precision degrades as SNR increases because more difficult targets are counted as hits, with less accurate peak localization. This trend is consistent with the lack of super-resolution in OMP and OLS, and with its only partial exploitation in OMP-iMUSIC. The

same behavior persists in the noiseless-limit regime, where SNR tends to infinity.

Consistently, Fig. 2b shows that precision degrades as K increases, in line with decreasing S and T . All methods coincide at $K = 1$, as expected for single-target estimation. As K grows, the precision gain of OLS-iMUSIC decreases, unlike the detection trend where gains become more visible at high K . This difference arises because precision is computed only over targets detected by all methods, which are typically the easiest ones.

Fig. 2c further shows that precision improves with the number of antennas M , as expected from the increase in T . As T increases, all methods improve similarly until they reach the resolution limit imposed by the discrete grid \mathcal{G}_θ (spacing $\sim 10^{-3}$). This behavior contrasts with the gain obtained by increasing S through larger Q . Specifically, increasing M (and thus improving T) benefits all methods, whereas increasing S benefits MUSIC-based and eigenvalue-criterion-based methods more strongly because they are more sensitive to inter-target signal correlation.

Overall, MUSIC and OLS-iMUSIC outperform OMP, OMP-iMUSIC, and OLS in precision. This behavior is expected because subspace methods such as MUSIC provide super-resolution. By contrast, OMP-iMUSIC does not reach

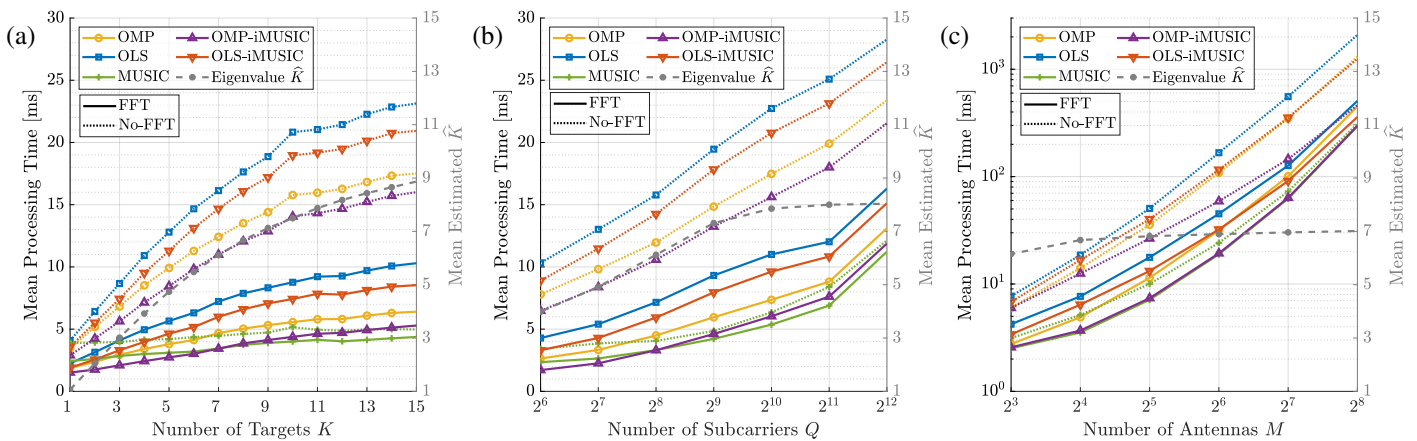


Fig. 3. Mean processing time versus (a) number of targets K , (b) number of subcarriers Q , and (c) number of antennas M . Solid lines denote FFT-accelerated implementations, whereas dotted lines denote non-accelerated implementations. In (c), the y-axis is logarithmic. The mean number of targets estimated by the eigenvalue-based criterion is also shown (dashed gray).

MUSIC-level precision because the greedy OMP framework does not solve the maximum likelihood (ML) least-squares problem at each iteration, which limits peak-localization accuracy. Therefore, OLS-iMUSIC tends to match the near-optimal precision of MUSIC by solving a least-squares problem at each iteration, whereas OMP-iMUSIC remains closer to OMP.

3) **Timing Performance:** We next evaluate timing performance by averaging the mean processing time of each algorithm, with and without FFT acceleration, across all simulations. As discussed in Section VI, we implement OMP and OLS using $\mathbf{R}_k^{1/2}$ rather than the observation matrix \mathbf{Y}_k because $DQ \gg M$ in the considered scenario. This choice substantially reduces processing time. Fig. 3 reports these results, where solid lines denote FFT-accelerated implementations and dotted lines denote non-accelerated implementations. To keep the comparison consistent, we show only the eigenvalue-based AIC criterion, so that all methods are compared under the same target-count estimate.

The observed timing trends are consistent with the theoretical complexity summary in Table II. In Fig. 3a, iterative-method runtime scales approximately linearly with K . However, this increase becomes weaker at high K because the eigenvalue-based AIC criterion saturates for large target counts [32]. By comparison, MUSIC is less sensitive to K because this parameter only changes subspace dimensions through K_M .

In Fig. 3b, the runtime of all methods scales linearly with the number of subcarriers Q . This trend is mainly driven by the increase in \mathcal{S} as Q grows, which improves the eigenvalue-based AIC criterion and thereby increases the number of detected targets across methods.

Fig. 3c shows that runtime scales quadratically with the number of antennas M . Here, the number of targets detected by the eigenvalue-based AIC criterion changes only marginally with M . Therefore, the dominant effect is the cost of evaluating the selection-step objective function, which scales as M^2 (or $M \log(M)$ with FFT acceleration) for OMP, OLS, and OMP-iMUSIC, and as M (or $\log(M)$ with FFT acceleration) for MUSIC and OLS-iMUSIC. Additionally, the EVD cost increases with M , which further contributes to the runtime

increase of all methods.

Overall, in agreement with the complexity analysis, G-iMUSIC methods are less computationally demanding than OMP and OLS, respectively. In addition, FFT acceleration significantly reduces processing time across all methods, with the largest gains for iterative methods, making them more suitable for real-time operation and competitive with MUSIC. At low K , OMP-iMUSIC can even be faster than MUSIC, because MUSIC requires a more expensive peak-detection stage, whereas OMP-iMUSIC uses a simple maximum search.

4) **G-iWMUSIC Performance:** For visual clarity, the curves of G-iWMUSIC methods in Figures 1, 2, and 3 are omitted. For detection and precision, the curves of OMP-iWMUSIC and OLS-iWMUSIC are superimposed on those of OMP and OLS, respectively. This overlap indicates that the low-rank approximation introduced by G-iWMUSIC does not degrade performance. For timing, their curves are superimposed on OMP-iMUSIC and OLS-iMUSIC, respectively, because weighting introduces a negligible computational overhead relative to unweighted variants. Therefore, G-iWMUSIC methods are fast alternatives to OMP and OLS, respectively, without performance degradation. However, in the considered scenario, they are outperformed by their non-weighted G-iMUSIC counterparts in terms of precision and detection performance.

VIII. CONCLUSION

In this paper, we presented novel G-iMUSIC algorithms for DoA estimation. These methods integrate the MUSIC subspace approach into the iterative greedy frameworks of OMP and OLS. Unlike existing iterative MUSIC approaches, the proposed methods adopt a principled greedy approach and avoid recomputing a new EVD at each iteration, thereby reducing computational cost. To further lower complexity, we also introduced FFT-based acceleration of the G-iMUSIC selection steps when a ULA is used.

Through numerical simulations, we demonstrated that the proposed OMP-iMUSIC and OLS-iMUSIC methods outperform their respective OMP and OLS baselines in terms of detection and precision, while also improving upon classical

MUSIC. In parallel, the complexity analysis showed that the proposed methods are less demanding than their OMP and OLS counterparts, with only limited additional overhead relative to MUSIC. The G-iWMUSIC variants provide low-rank approximations of the corresponding OMP and OLS selection steps, without performance degradation and with reduced computational cost. However, they are outperformed by their unweighted G-iMUSIC counterparts in the considered scenario. As a final contribution, we interpreted these outcomes using two diagnostic metrics, namely the steering-vector correlation metric (\mathcal{T}) and the signal correlation metric (\mathcal{S}), which provide scenario-agnostic insight into expected performance beyond the passive-radar setting considered here.

In conclusion, these results indicate that OMP-iMUSIC and OLS-iMUSIC offer an effective balance between estimation performance and complexity for real-time applications. The choice between the two variants can therefore be guided by the desired performance–complexity trade-off. Building on this foundation, future work will extend the proposed G-iMUSIC framework to other radar configurations, including Multiple-input and multiple-output (MIMO) and multistatic systems.

REFERENCES

- [1] M. Pesavento, M. Trinh-Hoang, and M. Viberg, “Three More Decades in Array Signal Processing Research: An optimization and structure exploitation perspective,” *IEEE Signal Processing Magazine*, vol. 40, no. 4, pp. 92–106, Jun. 2023.
- [2] A. A. Salama, “Direction of arrival estimation: A tutorial survey of classical and modern methods,” 2025. [Online]. Available: <https://arxiv.org/abs/2508.11675>
- [3] M. Pesavento and A. Gershman, “Maximum-likelihood direction-of-arrival estimation in the presence of unknown nonuniform noise,” *IEEE Transactions on Signal Processing*, vol. 49, no. 7, pp. 1310–1324, 2001.
- [4] M. K. B. Jeffrey Foutz, Andreas Spanias, *Narrowband Direction of Arrival Estimation for Antenna Arrays*. Springer Cham, 2008.
- [5] Y. Pati, R. Rezaifar, and P. Krishnaprasad, “Orthogonal matching pursuit: recursive function approximation with applications to wavelet decomposition,” in *Proceedings of 27th Asilomar Conference on Signals, Systems and Computers*, Nov. 1993, pp. 40–44 vol.1, iSSN: 1058-6393.
- [6] J. Tropp, “Greed is good: algorithmic results for sparse approximation,” *IEEE Transactions on Information Theory*, vol. 50, no. 10, pp. 2231–2242, Oct. 2004.
- [7] S. Chen, S. A. Billings, and W. Luo, “Orthogonal least squares methods and their application to non-linear system identification,” *International Journal of Control*, vol. 50, no. 5, pp. 1873–1896, Nov. 1989, publisher: Taylor & Francis, eprint: <https://doi.org/10.1080/00207178908953472>.
- [8] T. Blumensath and M. Davies, “On the Difference Between Orthogonal Matching Pursuit and Orthogonal Least Squares,” Mar. 2007.
- [9] S. Bourguignon, C. Soussen, H. Carfantan, and J. Idier, “Sparse deconvolution: Comparison of statistical and deterministic approaches,” in *2011 IEEE Statistical Signal Processing Workshop (SSP)*, Jun. 2011, pp. 317–320, iSSN: 2373-0803.
- [10] J. Wen, J. Li, H. Ge, Z. Zhou, and W. Luo, “Orthogonal Least Squares Detector for Generalized Spatial Modulation,” *IEEE Transactions on Wireless Communications*, vol. 20, no. 8, pp. 5071–5082, Aug. 2021.
- [11] S. Mukhopadhyay, P. V. and, and M. Chakraborty, “Signal Recovery in Uncorrelated and Correlated Dictionaries Using Orthogonal Least Squares,” Jul. 2016, arXiv:1607.08712 [cs].
- [12] C. Soussen, R. Gribonval, J. Idier, and C. Herzet, “Joint K-Step Analysis of Orthogonal Matching Pursuit and Orthogonal Least Squares,” *IEEE Transactions on Information Theory*, vol. 59, no. 5, pp. 3158–3174, May 2013.
- [13] M. Willame, G. Monnoyer, H. C. Yildirim, F. Horlin, and J. Louveaux, “Multi target localization with block orthogonal least squares for multistatic mimo radars,” *IEEE Signal Processing Letters*, vol. 32, pp. 1990–1994, 2025.
- [14] W. Rueckner and P. Costas, “How to beat the Rayleigh resolution limit: A lecture demonstration,” *American Journal of Physics*, vol. 70, no. 6, pp. 587–594, 2002.
- [15] R. Schmidt, “Multiple emitter location and signal parameter estimation,” *IEEE Transactions on Antennas and Propagation*, vol. 34, no. 3, pp. 276–280, 1986.
- [16] P. Stoica and A. Nehorai, “MUSIC, maximum likelihood, and cramer-rao bound: further results and comparisons,” *IEEE Transactions on Acoustics, Speech, and Signal Processing*, vol. 38, no. 12, pp. 2140–2150, 1990.
- [17] P. Gupta and S. Kar, “MUSIC and improved MUSIC algorithm to estimate direction of arrival,” in *2015 International Conference on Communications and Signal Processing (ICCSP)*, 2015, pp. 0757–0761.
- [18] M. Willame, H. C. Yildirim, L. Storrer, F. Horlin, and J. Louveaux, “Multistatic OFDM radar fusion of MUSIC-based angle estimation,” in *2024 18th European Conference on Antennas and Propagation (EuCAP)*, 2024, pp. 1–5.
- [19] Z. Tian, “Iterative MUSIC: Coherent signal estimation, performance analysis,” in *2002 IEEE International Conference on Acoustics, Speech, and Signal Processing*, vol. 3, 2002, pp. III–3041–III–3044.
- [20] N. Haddad, L. Harkati, K. Hadj-Rabab, A. Bouaraba, and A. Mesloub, “Iterative MUSIC for single-look SAR tomography,” in *2024 IEEE Mediterranean and Middle-East Geoscience and Remote Sensing Symposium (M2GARSS)*, 2024, pp. 201–204.
- [21] M. Shaghghi and S. A. Vorobyov, “Iterative root-MUSIC algorithm for DoA estimation,” in *2013 5th IEEE International Workshop on Computational Advances in Multi-Sensor Adaptive Processing (CAMSAP)*, 2013, pp. 53–56.
- [22] M. Zhou, H. Tian, and S. Fan, “DoA estimation with a combination of iterative MUSIC and SBL in low snr conditions,” in *2021 IEEE Wireless Communications and Networking Conference Workshops (WCNCW)*, 2021, pp. 1–6.
- [23] X. Zhang and D. Feng, “An efficient MUSIC algorithm enhanced by iteratively estimating signal subspace and its applications in spatial colored noise,” *Remote Sensing*, vol. 14, no. 17, 2022. [Online]. Available: <https://www.mdpi.com/2072-4292/14/17/4260>
- [24] L. Storrer, H. C. Yildirim, M. Crauwels, E. I. P. Copa, S. Pollin, J. Louveaux, P. De Doncker, and F. Horlin, “Indoor tracking of multiple individuals with an 802.11ax Wi-Fi-based multi-antenna passive radar,” *IEEE Sensors Journal*, vol. 21, no. 18, pp. 20462–20474, 2021.
- [25] I. Ziskind and M. Wax, “Maximum likelihood localization of multiple sources by alternating projection,” *IEEE Transactions on Acoustics, Speech, and Signal Processing*, vol. 36, no. 10, pp. 1553–1560, 1988.
- [26] M. A. Richards, J. A. Scheer, and W. A. Holm, “Principles of modern radar: Basic principles,” 2013. [Online]. Available: <https://api.semanticscholar.org/CorpusID:114114032>
- [27] R. Hunger, “Floating point operations in matrix-vector calculus.” *Tech. Rep.*, October 2005. [Online]. Available: <https://mediatum.ub.tum.de/doc/625604/625604>
- [28] G. Golub and C. Van Loan, *Matrix Computations*, ser. Johns Hopkins Studies in the Mathematical Sciences. Johns Hopkins University Press, 2013. [Online]. Available: <https://books.google.be/books?id=X5YfsuCWpxMC>
- [29] C. Donciu, M. C. Temneanu, and E. Serea, “Direct FFT oversampling without zero-padding,” *Scientific Reports*, vol. 15, 2025.
- [30] “IEEE standard for information technology–telecommunications and information exchange between systems local and metropolitan area networks–specific requirements - part 11: Wireless LAN medium access control (MAC) and physical layer (PHY) specifications amendment 2: Enhancements for extremely high throughput (EHT),” *IEEE Std 802.11be-2024 (Amendment to IEEE Std 802.11-2024, as amended by 802.11bh-2024)*, pp. 1–1020, 2025.
- [31] M. Wax and T. Kailath, “Detection of signals by information theoretic criteria,” *IEEE Transactions on Acoustics, Speech, and Signal Processing*, vol. 33, no. 2, pp. 387–392, 1985.
- [32] M. Willame, G. Monnoyer, F. Horlin, and J. Louveaux, “Orthogonal least squares with integrated information theoretic criteria for joint number of targets and doa estimation,” 2026. [Online]. Available: <https://arxiv.org/abs/2605.06198>
- [33] K. Alyani, M. Congedo, and M. Moakher, “Diagonality measures of hermitian positive-definite matrices with application to the approximate joint diagonalization problem,” *Linear Algebra and its Applications*, vol. 528, pp. 290–320, 2017, special Issue Dedicated to Rajendra Bhatia. [Online]. Available: <https://www.sciencedirect.com/science/article/pii/S0024379516303834>
- [34] H. W. Kuhn, *The Hungarian Method for the Assignment Problem*. Berlin, Heidelberg: Springer Berlin Heidelberg, 2010, pp. 29–47.
- [35] W. J. Youden, “Index for rating diagnostic tests,” *Cancer*, vol. 3, no. 1, pp. 32–35, 1950.

- [36] P. Martínez-Cambor and J. C. Pardo-Fernández, "The youden index in the generalized receiver operating characteristic curve context," *International Journal of Biostatistics*, vol. 15, 2019.